

1 **Technical note: on LA–ICP-MS U–Pb dating of unetched and etched apatites**

2 Fanis Abdullin et al.: LA–ICP-MS U–Pb dating of apatites

3 Fanis Abdullin¹, Luigi A. Solari², Jesús Solé³, Carlos Ortega-Obregón²

4 ¹CONACyT–Centro de Geociencias, Campus Juriquilla, UNAM, Querétaro, 76230, Mexico


5 ²Centro de Geociencias, Campus Juriquilla, UNAM, Querétaro, 76230, Mexico

6 ³LANGEM, Instituto de Geología, UNAM, Ciudad Universitaria, CDMX, 04510, Mexico


7 **Correspondence:** Fanis Abdullin (fanis@geociencias.unam.mx)

8

9 **Abstract**

10 The same unetched and chemically etched apatite grains from five rock samples were dated via 

11 U–Pb via laser ablation inductively-coupled plasma mass spectrometry (LA–ICP-MS). The

12 objective of this study is to ask  whether chemical etching required for apatite fission track

13 analysis impacts the precision and accuracy of ~~same-grain~~ U–Pb ages. The results of ~~our~~

14 experiment suggest that etching has ~~no~~ significant effect on the accuracy of apatite U–Pb ages

15 obtained by LA–ICP-MS. Thus, LA–ICP-MS ~~can be used safely for apatite fission track and U–~~

16 ~~Pb double dating.~~

17

18

19 **Short summary**

20 Unetched and etched apatite grains from five samples were dated ~~with~~ U–Pb using laser ablation

21 inductively-coupled plasma mass spectrometry. Our experiment indicates that etching needed for

22 apatite fission track dating has ~~no~~ effect on the obtaining accurate U–Pb ages; therefore, the laser

23 ablation-based technique may be used for apatite fission track and U–Pb double dating.

24

25 1 Introduction

26

27 Apatite, $\text{Ca}_5(\text{PO}_4)_3[\text{F},\text{Cl},\text{OH}]$, is the most common phosphate mineral in the Earth's crust and can
28 be found in practically all igneous and metamorphic rocks, in many ancient and recent sediments
29 as well as in certain mineral deposits (Piccoli and Candela, 2002; Morton and Yaxley, 2007;
30 Webster and Piccoli, 2015). This accessory mineral is often used as a natural thermochronometer
31 for fission track, He, U–Th and U–Pb dating (e.g., Zeitler et al., 1987; Wolf et al., 1996; Ehlers
32 and Farley, 2003; Hasebe et al., 2004; Donelick et al., 2005; Chew and Donelick, 2012; Chew et
33 al., 2014; Cochrane et al., 2014; Liu et al., 2014; Spikings et al., 2015; Glorie et al., 2017).
34 Presently, apatite fission track (AFT) ages can be obtained rapidly by using laser ablation
35 inductively-coupled plasma mass spectrometry (LA–ICP–MS) for direct measurement of “parent
36 nuclides”, i.e., ^{238}U contents (Cox et al., 2000; Svojtka and Košler, 2002; Hasebe et al., 2004,;
37 Donelick et al., 2005; Vermeesch, 2017). LA–ICP–MS technique may be used to obtain ^{238}U for
38 AFT dating, together with isotope ratios needed for U–Pb dating (e.g., Chew and Donelick,
39 2012; Liu et al., 2014; Glorie et al., 2017; Bonilla et al., 2020; Nieto-Samaniego et al., 2020).

40 Hasebe et al. (2009) previously performed an important experimental study, during which
41 they demonstrated that chemical etching required for fission track dating ~~has no significant effect~~
42 ~~on the accuracy of U measurement by LA–ICP–MS method~~. After chemical etching of apatites, a
43 smaller volume of ablated material is analyzed by LA–ICP–MS. The influence of etching needed
44 for AFT dating on the precision and accuracy of ~~same-grain U–Pb dating analyzed~~ via LA–ICP–
45 MS remains to be quantified. To investigate this issue, the same unetched and etched apatite
46 grains extracted from five rock samples were analyzed using LA–ICP–MS for U–Pb dating. The

47 chosen rock samples have either emplacement or metamorphic ages ranging from the Cretaceous
48 to the Neoproterozoic (see Table 1 for further details).

49 --- **Table 1** ---

50

51


52

53 **2 Sample descriptions**

54

55 2.1 OV-0421 (Tres Sabanas Pluton, Guatemala)

56

57 This sample is a two mica-bearing deformed granite belonging to the Tres Sabanas Pluton, which
58 is located  of Guatemala City, Guatemala. For sample OV-0421, an emplacement age of 115
59 ± 4 (2σ) Ma was proposed based on zircon U–Pb data (Torres de León, 2016). A cooling age of
60 102 ± 1 (2σ) Ma, obtained with K–Ar (on biotite), ~~has also been~~ reported by the same author.

61

62 2.2. MCH-38 (Chiapas Massif Complex, Mexico)

63

64 MCH-38 is an orthogneiss from the Permian Chiapas Massif Complex. This rock was sampled to
65 the west of Unión Agrarista, the State of Chiapas, southeastern Mexico. There is no reported age
66 for this sample. Some zircon U–Pb dates obtained for the Chiapas Massif Complex (Weber et al.,
67 2007, 2008; Ortega-Obregón et al., 2019) suggest that a Lopingian (260–252 Ma) crystallization
68 or metamorphic age may be assumed for sample MCH-38.

69

70 2.3 TO-AM (Totoltepec Pluton, Mexico)

71

72 TO-AM is a granitic rock, sampled ca. 5 km west of Totoltepec de Guerrero, the State of Puebla,
73 southern Mexico. There is no reported radiometric data for sample TO-AM. Previous geological
74 studies indicate that the Pennsylvanian–Cisuralian Totoltepec Pluton was emplaced over a ca. 23
75 million year period (from ca. 308 to ca. 285 Ma; e.g., Kirsch et al., 2013).

76

77 2.4 CH-0403 (Altos Cuchumatanes, Guatemala)

78

79 CH-0403 was collected 5 km ESE of Barillas, in the Altos Cuchumatanes, Guatemala. It consists
80 of a gray to green granodiorite. Five zircon aliquots of sample CH-0403 were dated using isotope
81 dilution thermal-ionization mass spectrometry, yielding a lower intercept date of 391 ± 8 (2σ)
82 Ma that is interpreted as its approximate crystallization age (Solari et al., 2009).

83

84 2.5 OC-1008 (Oaxacan Complex, Mexico)

85

86 This sample is a paragneiss from the Grenvillian Oaxacan Complex, southern Mexico. OC-1008
87 was collected in the federal road which connects Nochixtlán to Oaxaca. It was demonstrated that
88 this sample underwent granulite facies metamorphism at 1000–980 Ma (Solari et al., 2014).

89

90

91

92

93 3 Analytical procedures

94

95 Accessory minerals were concentrated using conventional mineral separation techniques such as
96 rock crushing, sieving, Wilfley table, Frantz magnetic separator, and bromoform. Approximately
97 300 apatite grains were extracted from each rock sample and mounted with their surfaces parallel
98 to the crystallographic *c*-axis in a 2.5 cm diameter epoxy mount. Mounted crystals were polished
99 to expose their internal surfaces (i.e., up to 4π geometry). For this experiment, complete crystals
100 lacking visible inclusions and other defects, such as cracks, were carefully selected for analysis.
101 Sample preparation was performed at Taller de Molienda and Taller de Laminación, Centro de
102 Geociencias (CGEO), Campus Juriquilla, Universidad Nacional Autónoma de Mexico (UNAM).

103 Single spot analyses were performed with a Resonetics RESolution™ LPX Pro (193 nm,
104 ArF excimer) laser ablation system, coupled to a Thermo Scientific iCAP™ Qc quadrupole ICP-
105 MS at Laboratorio de Estudios Isotópicos (LEI), CGEO, UNAM. During this experimental work,
106 LA–ICP-MS-based sampling was performed in central parts of the selected apatite grains before
107 and after chemical etching (in 5.5M HNO₃ at 21 °C for 20 s to reveal spontaneous fission tracks),
108 as shown schematically in Fig. 1. The LA–ICP-MS protocol used for apatite analyses, as given in
109 Table 2, was established on the basis of numerous experiments carried out at LEI during the past
110 five years, and can be used for U–Pb and fission track double dating plus multielemental analysis
111 (Abdullin et al., 2018; Ortega-Obregón et al., 2019). Corrected isotopic ratios and errors were
112 calculated using Iolite 3.5 (Paton et al., 2011) and the VizualAge data reduction scheme (Petrus
113 and Kamber, 2012). UcomPbine (Chew et al., 2014) was used to model ²⁰⁷Pb/²⁰⁶Pb initial values
114 and thus force a ²⁰⁷Pb correction that considers the common Pb (non-radiogenic Pb) incorporated
115 by apatite standards at the moment of their crystallization (see also Ortega-Obregón et al., 2019).

116 The “First Mine Discovery” apatite from Madagascar, with a mean U–Pb age of ca. 480 Ma
117 (Thomson et al., 2012; Chew et al., 2014), was used as a primary reference material. The results
118 for measured isotopes using NIST-612 (Pearce et al., 1997) were normalized using ^{43}Ca as an
119 internal standard and taking an average CaO content of 55% (i.e., for F-apatites).

120 Tera and Wasserburg Concordia diagrams (T–W; Tera and Wasserburg, 1972) are used in
121 apatite U–Pb dating, because the LA–ICP–MS-derived U–Pb results are generally discordant.
122 The lower intercept in the T–W plot is considered as a mean apatite U–Pb age that should have
123 geological significance (crystallization or cooling age, the age of mineralization or metamorphic
124 event). Apatite U–Pb ages were calculated with IsoplotR (Vermeesch, 2017, 2018) and described
125 below. Detailed information on our U–Pb experiments is given in Table S1 in the Supplement.

126 --- **Figure 1** ---

127 --- **Table 2** ---

128

129

130 **4 Results**

131

132 4.1 OV-0421

133

134 For rock sample OV-0421, 41 unetched apatites yielded a lower intercept age of 106 ± 4 (2σ) Ma
135 with a mean square weighted deviation (MSWD) of 1.07, passing the chi-squared test with the
136 $P(\chi^2)$ value of 0.35 (see in Fig. 2). Virtually the same U–Pb date, 107 ± 5 (2σ) Ma, was obtained
137 after chemical etching of the same apatite grains, yielding a MSWD of 1.13 and a $P(\chi^2)$ of 0.27.
138 Both these apatite U–Pb ages lie between the zircon U–Pb date of 115 ± 4 (2σ) Ma (i.e.,

139 crystallization age) and the biotite K–Ar age of 102 ± 1 (2σ) Ma (i.e., cooling age), which were
140 previously obtained for the same granite sample by Torres de León (2016).

141

142 4.2. MCH-38

143

144 For orthogneiss sample MCH-38, the lower intercept in T–W yielded a U–Pb age of 245 ± 6 (2σ)
145 Ma (obtained from 41 unetched apatites) with a MSWD of 0.28 and a $P(\chi^2)$ of 1. Etched apatite
146 grains from MCH-38 yielded an age of 240 ± 4 (2σ) Ma with a MSWD of 0.36 and a $P(\chi^2)$ of 1
147 (Fig. 2). Our U–Pb results are in close agreement with geochronological data reported from the
148 Chiapas Massif Complex in previous studies (Damon et al., 1981; Torres et al., 1999; Schaaf et
149 al., 2002; Ortega-Obregón et al., 2019). For instance, Torres et al. (1999) compiled biotite K–Ar
150 ages, most of which lie within Early–Middle Triassic period. Triassic cooling ages in the Chiapas
151 Massif Complex were also detected by Rb–Sr in mica–whole rock pairs that range from 244 ± 12
152 (2σ) Ma to 214 ± 11 (2σ) Ma (Schaaf et al., 2002).

153

154 4.3 TO-AM

155

156 Unetched apatites (32 crystals; Fig. 2) from granite TO-AM yielded a lower intercept date of 303
157 ± 5 (2σ) Ma with a MSWD of 0.6 and a $P(\chi^2)$ of 0.96. After etching, a slightly younger age of
158 299 ± 3 (2σ) Ma was obtained, with a MSWD of 0.89 and a $P(\chi^2)$ of 0.65. These apatite U–Pb
159 ages are in line with the zircon U–Pb ages of 306 ± 2 (2σ) Ma to 287 ± 2 (2σ) Ma reported for
160 the Pennsylvanian–Cisuralian Totoltepec Pluton (e.g., see details in Kirsch et al., 2013).

161

162 4.4 CH-0403

163

164 36 unetched apatite grains from sample CH-0403 yielded a lower intercept U–Pb age of 345 ± 10
165 (2σ) Ma with a MSWD of 0.7 and a $P(\chi^2)$ of 0.9, whereas etched grains yielded an age of 334 ± 8
166 (2σ) Ma with a MSWD of 1.37 and a $P(\chi^2)$ of 0.08 (Fig. 2). These cooling dates are considerably
167 younger if compared to the CH-0403 emplacement age of 391 ± 8 (2σ) Ma (Solari et al., 2009).

168

169 4.5 OC-1008

170

171 41 unetched apatites belonging to the sample OC-1008 yielded a U–Pb age of 839 ± 12 (2σ) Ma
172 with a MSWD of 0.98 and a $P(\chi^2)$ of 0.50. After etching, the same apatite crystals yielded an age
173 of 830 ± 10 (2σ) Ma with a MSWD of 1.24 and a $P(\chi^2)$ of 0.14 (Fig. 2). Both these apatite U–Pb
174 ages are significantly younger than the age of granulite facies metamorphism in the Grenville-
175 aged Oaxacan Complex (1 Ga to 980 Ma, Solari et al., 2014), and thus, should be considered as
176 cooling ages.

177

--- Figure 2 ---

178

179

180 **5 Discussion and concluding remarks**

181

182 Most rock samples, except OV-0421, yielded slightly younger apatite U–Pb ages after chemical
183 etching (up to 3.3% in sample CH-0403). However, the lower intercept U–Pb ages obtained from
184 unetched apatite grains are identical within errors to the U–Pb ages obtained on the same etched

185 grains (see diagram in Fig. 3). The results of ~~our experimental study~~ demonstrate that ~~the~~
186 chemical etching, required for ~~the~~ AFT analysis, has ~~no important~~ effect on the accuracy of
187 apatite U–Pb ages determined via LA–ICP-MS. Thus, as a main conclusion of this ~~experimental~~
188 study, LA–ICP-MS can be used ~~safely to obtain~~ simultaneously AFT and U–Pb ages (~~i.e., double~~
189 ~~dating~~), as it was already done in ~~some~~ studies ~~without previous proof~~ (e.g., Chew and Donelick,
190 2012; Liu et al., 2014; Glorie et al., 2017; Bonilla et al., 2020; Nieto-Samaniego et al., 2020).

191 --- **Figure 3** ---

192

193 **Supplement**

194 The supplement related to this article is available online at: <https://...>

195

196 **Author contributions**

197 Conceptualisation, investigation, and writing of the original draft were done by FA. LS and COO
198 provided technical support. LS and JS acquired funding and resources, supervised the study, and
199 reviewed the manuscript.

200

201 **Competing interests**

202 The authors declare that they have no conflict of interest.

203

204

205

206

207

208 **Acknowledgements**

209 The authors are grateful to Juan Tomás Vázquez Ramírez and Ofelia Pérez Arvizu for their help
210 with sample preparation for this study. Professor Stuart Thomson is acknowledged for sharing
211 Madagascar apatite. Dr. Michelangelo Martini kindly provided sample TO-AM that was useful
212 for our experimental study. Dr. Ziva Shulaker, Dr. Jakub Sliwinski, and Professor Axel Schmitt
213 are acknowledged for their constructive comments that improved our manuscript.

214

215 **Financial support**

216 This research has been supported by PAPIIT DGAPA UNAM (grant no. IN101520 to LS).

217

218 **Figure caption**

219

220 **Figure 1**

221 Illustration displaying the LA-ICP-MS-based U-Pb dating of the same apatite crystal before and
222 after chemical etching (i.e., etched in 5.5M nitric acid at 21 °C for 20 s). Spot diameter of 60 µm.

223

224 **Figure 2**

225 Tera-Wasserburg Concordia diagrams for the U-Pb results of unetched and etched apatites from
226 samples OV-0421, MCH-38, TO-AM, CH-0403, and OC-1008. MSWD – mean square weighted
227 deviation, Ngr – number of grains dated. Errors are given in 2σ .

228

229 **Figure 3**

230 Plot showing the lower intercept U-Pb ages obtained on unetched and etched apatite grains.

231
232
233
234
235
236
237
238
239
240
241
242
243
244
245
246
247
248
249
250
251
252
253

References

Abdullin, F., Solari, L., Ortega-Obregón, C., and Solé, J.: New fission-track results from the northern Chiapas Massif area, SE Mexico: trying to reconstruct its complex thermo-tectonic history, *Revista Mexicana de Ciencias Geológicas*, 35, 79–92, <https://doi.org/10.22201/cgeo.20072902e.2018.1.523>, 2018.

Bonilla, A., Franco, J. A., Cramer, T., Poujol, M., Cogné, N., Nachtergaele, S., and De Grave, J.: Apatite LA-ICP-MS U–Pb and fission-track geochronology of the Caño Viejita gabbro in E-Colombia: Evidence for Grenvillian intraplate rifting and Jurassic exhumation in the NW Amazonian Craton, *Journal of South American Earth Sciences*, 98, 102438, <https://doi.org/10.1016/j.jsames.2019.102438>, 2020.

Chew, D. M., and Donelick, R. A.: Combined apatite fission track and U-Pb dating by LA-ICP-MS and its application in apatite provenance analysis, *Quantitative Mineralogy and Microanalysis of Sediments and Sedimentary Rocks: Mineralogical Association of Canada, Short Course*, 42, 219–247, 2012.

Chew, D. M., Petrus, J. A., and Kamber, B. S.: U–Pb LA–ICPMS dating using accessory mineral standards with variable common Pb, *Chemical Geology*, 363, 185–199, <https://doi.org/10.1016/j.chemgeo.2013.11.006>, 2014.

254
255
256
257
258
259
260
261
262
263
264
265
266
267
268
269
270
271
272
273
274
275
276

Cochrane, R., Spikings, R. A., Chew, D., Wotzlaw, J. F., Chiaradia, M., Tyrrell, S., Schaltegger, U., and Van der Lelij, R.: High temperature ($> 350\text{ }^{\circ}\text{C}$) thermochronology and mechanisms of Pb loss in apatite, *Geochimica et Cosmochimica Acta*, 127, 39–56, <https://doi.org/10.1016/j.gca.2013.11.028>, 2014.

Cox, R., Košler, J., Sylvester, P., and Hodych, P.: Apatite fission-track (FT) dating by LAM-ICP-MS analysis, Goldschmidt Conference, Oxford, UK, *Journal of Conference Abstracts*, 5, p. 322, 2000.

Damon, P. E., Shafiqullah, M., and Clark, K. F.: Age trends of igneous activity in relation to metallogenesis in the southern Cordillera, Tucson, Arizona, *Arizona Geological Society Digest*, 14, 137–153, 1981.

Donelick, R. A., O’Sullivan, P. B., and Ketcham, R. A.: Apatite fission-track analysis, *Reviews in Mineralogy and Geochemistry*, 58, 49–94, <https://doi.org/10.2138/rmg.2005.58.3>, 2005.

Ehlers, T. A., and Farley, K. A.: Apatite (U–Th)/He thermochronometry: methods and applications to problems in tectonic and surface processes, *Earth and Planetary Science Letters*, 206, 1–14, [https://doi.org/10.1016/S0012-821X\(02\)01069-5](https://doi.org/10.1016/S0012-821X(02)01069-5), 2003.

277 Glorie, S., Alexandrov, I., Nixon, A., Jepson, G., Gillespie, J., and Jahn, B. M.: Thermal and
278 exhumation history of Sakhalin Island (Russia) constrained by apatite U-Pb and fission track
279 thermochronology, *Journal of Asian Earth Sciences*, 143, 326–342,
280 <https://doi.org/10.1016/j.jseaes.2017.05.011>, 2017.

281

282 Hasebe, N., Barbarand, J., Jarvis, K., Carter, A., and Hurford, A. J.: Apatite fission-track
283 chronometry using laser ablation ICP-MS, *Chemical Geology*, 207, 135–145,
284 <https://doi.org/10.1016/j.chemgeo.2004.01.007>, 2004.

285

286 Hasebe, N., Carter, A., Hurford, A. J., and Arai, S.: The effect of chemical etching on LA-ICP-
287 MS analysis in determining uranium concentration for fission-track chronometry, *Geological*
288 *Society, London, Special Publications*, 324, 37–46, <https://doi.org/10.1144/SP324.3>, 2009.

289

290 Kirsch, M., Keppie, J. D., Murphy, J. B., and Lee, J. K.: Arc plutonism in a transtensional
291 regime: the late Palaeozoic Totoltepec pluton, Acatlán Complex, southern Mexico, *International*
292 *Geology Review*, 55, 263–286, <https://doi.org/10.1080/00206814.2012.693247>, 2013.

293

294 Liu, W., Zhang, J., Sun, T., Wang, J.: Application of apatite U–Pb and fission-track double
295 dating to determine the preservation potential of magnetite–apatite deposits in the Luzong and
296 Ningwu volcanic basins, eastern China, *Journal of Geochemical Exploration*, 138, 22–32,
297 <https://doi.org/10.1016/j.gexplo.2013.12.006>, 2014.

298

299

300 Morton, A., and Yaxley, G.: Detrital apatite geochemistry and its application in provenance
301 studies, *Special Papers, Geological Society of America*, 420, 319,
302 [https://doi.org/10.1130/2006.2420\(19\)](https://doi.org/10.1130/2006.2420(19)), 2007.

303

304 Nieto-Samaniego, A. F., Olmos-Moya, M. D. J. P., Levresse, G., Alaniz-Alvarez, S. A.,
305 Abdullin, F., del Pilar-Martínez, A., and Xu, S.: Thermochronology and exhumation rates of
306 granitic intrusions at Mesa Central, Mexico, *International Geology Review*, 62, 311–319,
307 <https://doi.org/10.1080/00206814.2019.1602789>, 2020.

308

309 Ortega-Obregón, C., Abdullin, F., Solari, L., Schaaf, P., and Solís-Pichardo, G.: Apatite U-Pb
310 dating at UNAM laboratories: analytical protocols and examples of its application, *Revista*
311 *Mexicana de Ciencias Geológicas*, 36, 27–37,
312 <https://doi.org/10.22201/cgeo.20072902e.2019.1.749>, 2019.

313

314 Paton, C., Hellstrom, J., Paul, B., Woodhead, J., Hergt, J.: Iolite: Freeware for the visualisation
315 and processing of mass spectrometric data, *Journal of Analytical Atomic Spectrometry*, 26,
316 2508–2518, <https://doi.org/10.1039/C1JA10172B>, 2011.

317

318 Pearce, N. J., Perkins, W. T., Westgate, J. A., Gorton, M. P., Jackson, S. E., Neal, C. R., and
319 Chenery, S. P.: A compilation of new and published major and trace element data for NIST SRM
320 610 and NIST SRM 612 glass reference materials, *Geostandards newsletter*, 21, 115–144,
321 <https://doi.org/10.1111/j.1751-908X.1997.tb00538.x>, 1997.

322

323

324 Petrus, J. A., and Kamber, B. S.: VizualAge: A novel approach to laser ablation ICP-MS U-Pb
325 geochronology data reduction, *Geostandards and Geoanalytical Research*, 36, 247–270,
326 <https://doi.org/10.1111/j.1751-908X.2012.00158.x>, 2012.

327

328 Piccoli, P. M., and Candela, P. A.: Apatite in igneous systems, *Reviews in Mineralogy and*
329 *Geochemistry*, 48, 255–292, <https://doi.org/10.2138/rmg.2002.48.6>, 2002.

330

331 Schaaf, P., Weber, B., Weis, P., Groß, A., Ortega-Gutiérrez, F., and Kohler, H.: The Chiapas
332 Massif (Mexico) revised: New geologic and isotopic data and basement characteristics, *Neues*
333 *Jahrbuch für Geologie und Paläontologie, Abhandlungen*, 225, 1–23, 2002.

334

335 Solari, L. A., Ortega-Gutiérrez, F., Elías-Herrera, M., Schaaf, P., Norman, M., Ortega-Obregón,
336 C., and Chiquín, M.: U-Pb zircon geochronology of Palaeozoic units in western and central
337 Guatemala: Insights into the tectonic evolution of Middle America, *Geological Society, London,*
338 *Special Publications*, 328, 295–313, <https://doi.org/10.1144/SP328.12>, 2009.

339

340 Solari, L. A., Ortega-Gutiérrez, F., Elías-Herrera, M., Ortega-Obregón, C., Macías-Romo, C.,
341 Reyes-Salas, M.: Detrital provenance of the Grenvillian Oaxacan Complex, southern Mexico: a
342 zircon perspective, *International Journal of Earth Sciences*, 103, 1301–1315,
343 <https://doi.org/10.1007/s00531-013-0938-9>, 2014.

344

345

346 Spikings, R., Cochrane, R., Villagomez, D., Van der Lelij, R., Vallejo, C., Winkler, W., and
347 Beate, B.: The geological history of northwestern South America: From Pangaea to the early
348 collision of the Caribbean large igneous province (290–75 Ma), *Gondwana Research*, 27, 95–
349 139, <https://doi.org/10.1016/j.gr.2014.06.004>, 2015.

350

351 Svojtka, M., and Košler: Fission-track dating of zircon by LA-ICP-MS, Goldschmidt
352 Conference, Davos, Switzerland, *Journal of Conference Abstracts, Special Supplement of*
353 *Geochimica et Cosmochimica Acta*, 66, A756, 2002.

354

355 Tera, F., and Wasserburg, G. J.: U-Th-Pb systematics in three Apollo 14 basalts and the problem
356 of initial Pb in lunar rocks, *Earth and Planetary Science Letters*, 14, 281–304,
357 [https://doi.org/10.1016/0012-821X\(72\)90128-8](https://doi.org/10.1016/0012-821X(72)90128-8), 1972.

358

359 Thomson, S. N., Gehrels, G. E., Ruiz, J., and Buchwaldt, R.: Routine low-damage apatite U-Pb
360 dating using laser ablation–multicollector–ICPMS, *Geochemistry, Geophysics, Geosystems*,
361 13(2), <https://doi.org/10.1029/2011GC003928>, 2012.

362

363 Torres, R., Ruiz, J., Patchett, P. J., Grajales, J. M., Bartolini, C., Wilson, J. L., and Lawton, T. F.:
364 Permo-Triassic continental arc in eastern Mexico: Tectonic implications for reconstruction of
365 southern North America, *Geological Society of America, Special Papers*, 340, 191–196,
366 <https://doi.org/10.1130/0-8137-2340-X.191>, 1999.

367

368

369 Torres de León, R.: Caracterización geológica y geocronológica de unidades metamórficas e
370 intrusivas de la región centro-Oeste de la Cuenca del Río Motagua, Sureste de Guatemala,
371 Centroamerica: implicaciones en las conexiones Sur de México–Bloque Chortís, Universidad
372 Nacional Autónoma de México, Posgrado en Ciencias de la Tierra, Ph.D Thesis, 221 pp., 2016.
373

374 Vermeesch, P.: Statistics for LA-ICP-MS based fission track dating, *Chemical Geology*, 456,
375 19–27, <https://doi.org/10.1016/j.chemgeo.2017.03.002>, 2017.
376

377 Vermeesch, P.: IsoplotR: A free and open toolbox for geochronology, *Geoscience Frontiers*, 9,
378 1479–1493, <https://doi.org/10.1016/j.gsf.2018.04.001>, 2018.
379

380 Weber, B., Iriando, A., Premo, W. R., Hecht, L., and Schaaf, P.: New insights into the history
381 and origin of the southern Maya block, SE Mexico: U–Pb–SHRIMP zircon geochronology from
382 metamorphic rocks of the Chiapas massif, *International Journal of Earth Sciences*, 96, 253–269,
383 <https://doi.org/10.1007/s00531-006-0093-7>, 2007.
384

385 Weber, B., Valencia, V. A., Schaaf, P., Pompa-Mera, V., and Ruiz, J.: Significance of
386 provenance ages from the Chiapas Massif Complex (southeastern Mexico): redefining the
387 Paleozoic basement of the Maya Block and its evolution in a peri-Gondwanan realm, *The*
388 *Journal of Geology*, 116, 619–639, <https://doi.org/10.1086/591994>, 2008.
389

390 Webster, J. D., and Piccoli, P. M.: Magmatic apatite: A powerful, yet deceptive, mineral,
391 *Elements*, 11, 177–182, <https://doi.org/10.2113/gselements.11.3.177>, 2015.

392

393 Wolf, R. A., Farley, K. A., and Silver, L. T.: Helium diffusion and low-temperature
394 thermochronometry of apatite, *Geochimica et Cosmochimica Acta*, 60, 4231–4240,
395 [https://doi.org/10.1016/S0016-7037\(96\)00192-5](https://doi.org/10.1016/S0016-7037(96)00192-5), 1996.

396

397 Zeitler, P. K., Herczeg, A. L., McDougall, I., and Honda, M.: U-Th-He dating of apatite: A
398 potential thermochronometer, *Geochimica et Cosmochimica Acta*, 51, 2865–2868,
399 [https://doi.org/10.1016/0016-7037\(87\)90164-5](https://doi.org/10.1016/0016-7037(87)90164-5), 1987.

400

401

402

403

404

405

406

407

408

409

410

411

412

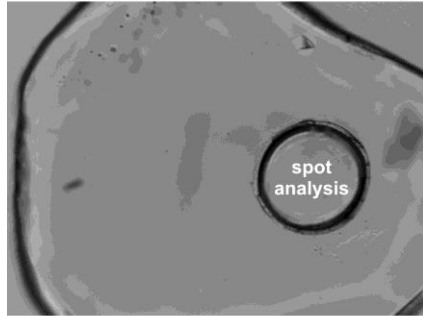
413

414

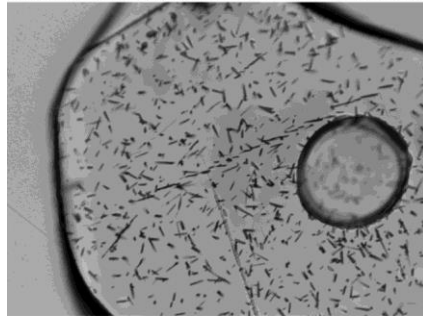
415

Figure 1

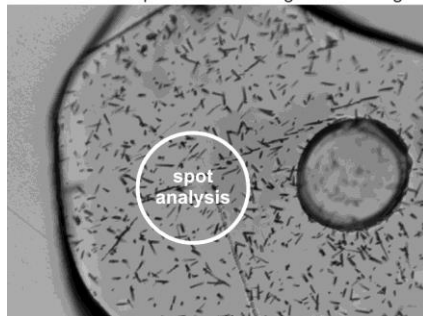
LA-ICP-MS apatite U-Pb dating before etching



chemical etching (5.5M nitric acid, 21 °C for 20 s)



LA-ICP-MS apatite U-Pb dating after etching



416

417

418

419

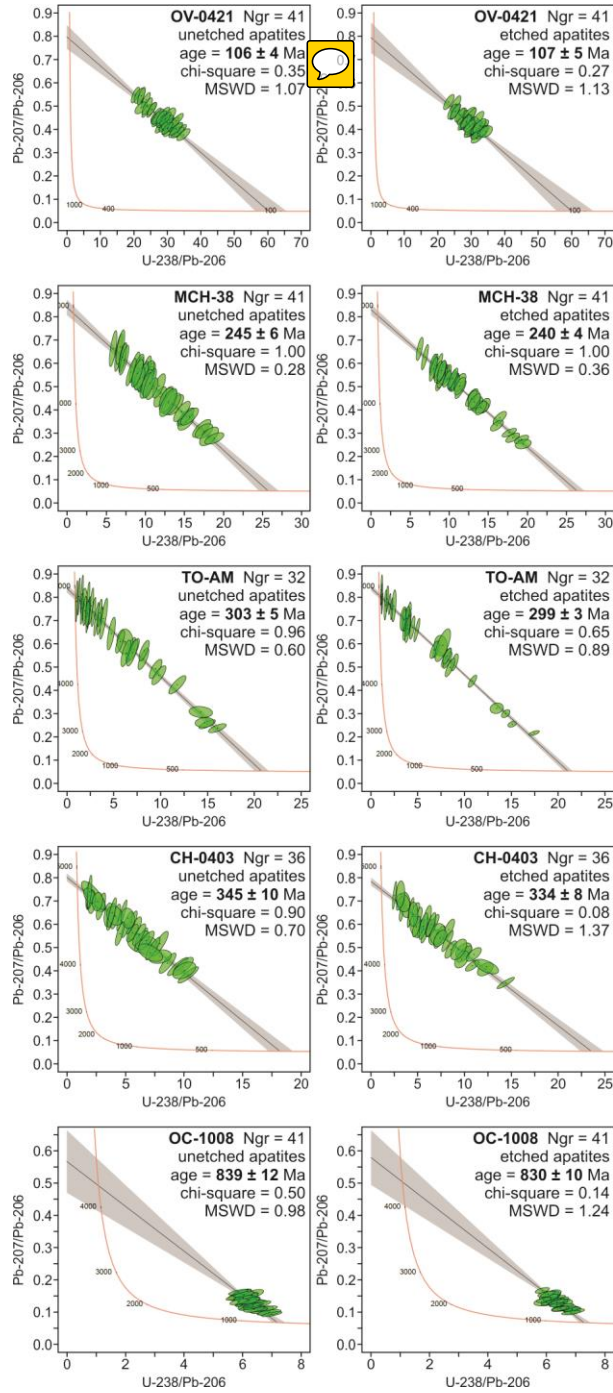
420

421

422

423

Figure 2



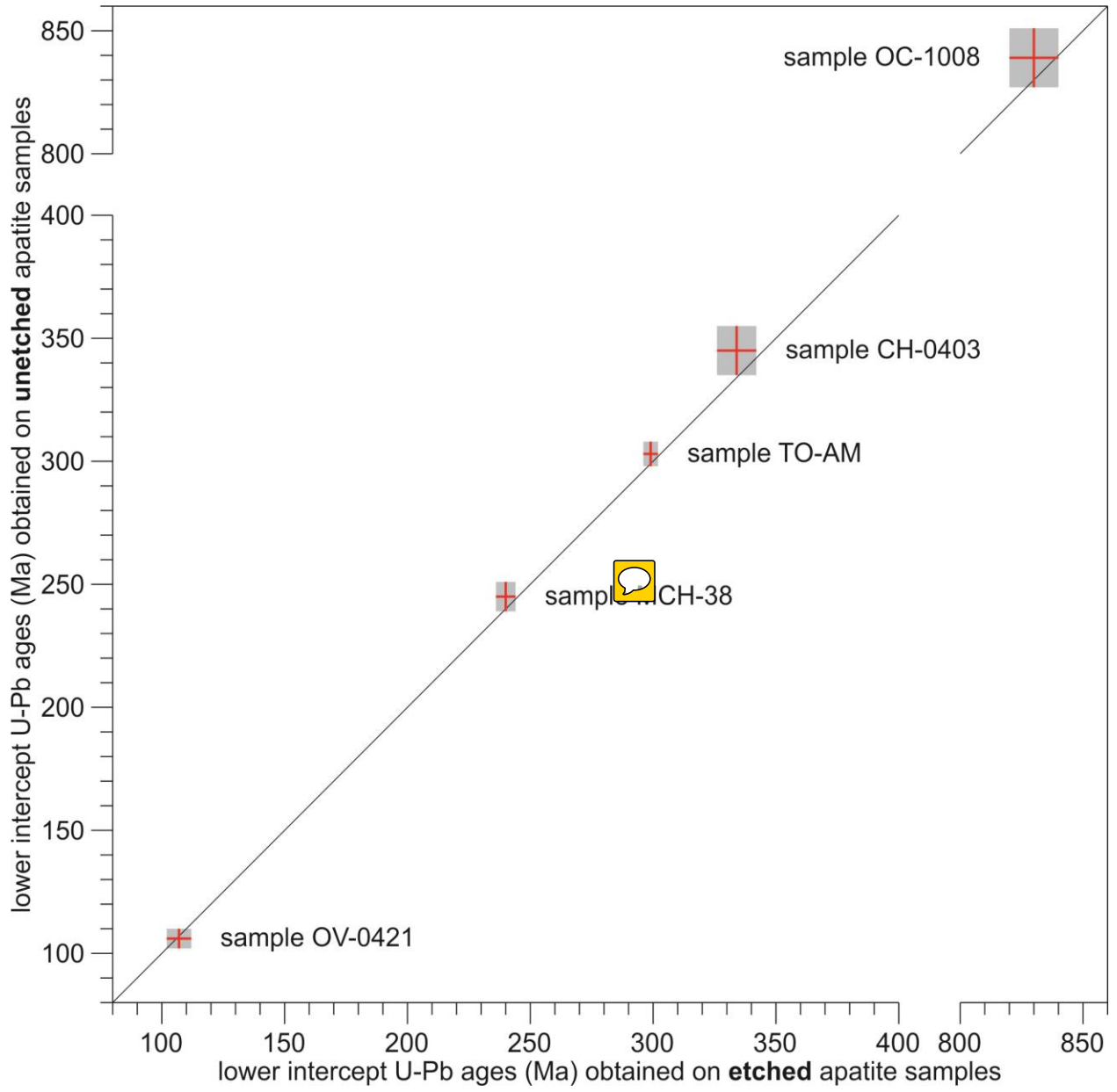
425

426

427

428

Figure 3



430

431

432

433

434

435

436

437 **Table 1**

438

439 Lithology, locality, and zircon U–Pb data for the selected experimental rock samples.

Sample	Unit and locality	Rock type	Zircon U–Pb age	References
OV-0421	Tres Sabanas Pluton, Guatemala	deformed granite	115 ± 4 Ma	Torres de León (2016)
MCH-38	Chiapas Massif Complex, Mexico	orthogneiss	ca. 260 to ca. 252 Ma (?)	Weber et al. (2007, 2008)
TO-AM	Totoltepec Pluton, Mexico	granite	ca. 308 to ca. 285 Ma (?)	Kirsch et al. (2013)
CH-0403	Altos Cuchumatanes, Guatemala	granodiorite	391 ± 8 Ma	Solari et al. (2009)
OC-1008	Oaxacan Complex, Mexico	paragneiss	990 ± 10 Ma	Solari et al. (2014)

440

441

442

443

444

445

446

447

448

449

450

451

452

453

454

455

456 **Table 2**

457

458 LA-ICP-MS protocol established at LEI to be applied for simultaneous apatite U-Pb and fission-
 459 track *in-situ* double dating plus multielemental analysis (REEs, Y, Sr, Mn, Mg, Th, U, and Cl).

<i>ICP-MS operating conditions</i>	
Instrument	Thermo Scientific™ iCAP™ Qc
Forward power	1450 W
Carrier gas flow rate	~1 L/min (Ar) and ~0.35 L/min (He)
Auxiliary gas flow rate	~1 L/min
Plasma gas flow rate	~14 L/min
Nitrogen	~3.5 mL/min
<i>Data acquisition parameters</i>	
Mode of operating	STD (standard mode)
Sampling scheme	-2NIST-612-2MAD-1DUR-10apt-
Background scanning	15 s
Data acquisition time	35 s
Wash-out time	15 s
Measured isotopes	²⁶ Mg ³¹ P ³⁵ Cl ⁴³ Ca ⁴⁴ Ca ⁵⁵ Mn ⁸⁸ Sr ⁸⁹ Y ¹³⁹ La ¹⁴⁰ Ce ¹⁴¹ Pr ¹⁴⁶ Nd ¹⁴⁷ Sm ¹⁵³ Eu ¹⁵⁷ Gd ¹⁵⁹ Tb ¹⁶³ Dy ¹⁶⁵ Ho ¹⁶⁶ Er ¹⁶⁹ Tm ¹⁷² Yb ¹⁷⁵ Lu ²⁰² Hg ²⁰⁴ Pb ²⁰⁶ Pb ²⁰⁷ Pb ²⁰⁸ Pb ²³² Th ²³⁸ U [total = 29]
<i>Laser ablation system</i>	
Ablation cell	RESolution™ Laurin Technic S-155
Model of laser	Resonetics RESolution™ LPX Pro
Wavelength	193 nm (Excimer ArF)
Repetition rate	4 Hz
Energy density	*4 J/cm ²
Mode of sampling	spot diameter of 60 μm

460

461 Note: MAD – “First mine Discovery” U-Pb apatite standard from Madagascar; DUR – Durango
 462 apatite from Cerro de Mercado mine (Mexico); apt – unknown apatite crystals. (*) Laser pulse
 463 energy of 4 J/cm², which was measured directly on target with a Coherent™ laser energy meter.

464